Available online at www.sciencedirect.com

SCIENCE DIRECT®

Journal of Volcanology and Geothermal Research 142 (2005) 1–9

Journal of volcanology and geothermal research

www.elsevier.com/locate/jvolgeores

Welding processes in volcanology: insights from field, experimental, and modeling studies

Anita Grunder[a,*], J.K. Russell[b]

[a]Department of Geosciences, Oregon State University, Corvallis, OR, USA
[b]Igneous Petrology Laboratory, Department of Earth and Ocean Sciences, University of British Columbia, Vancouver, British Columbia, Canada V6T 1Z4

Received 16 July 2004; accepted 8 October 2004

Abstract

This volume is a collection of ten papers largely derived from a special session, Welding Processes in Volcanology, organized for the 2003 meeting of EUG-EGS-AGU in Nice, France, and brings together field, experimental, and modeling studies. We briefly review advances in understanding welding as represented by this volume and point to future lines of inquiry, with an emphasis on understanding the timescales of welding, the metrics of strain, and feedback relationships between compaction, porosity, permeability loss, fluid transport and rheology of the deposit. Our analysis suggests that, within the realm of field and textural studies, more systematic and quantitative data are necessary to evaluate strain histories related to welding and the timing of welding relative to other processes during eruption and emplacement. A new generation of experiments is needed in which load, strain rate and volatile pressure can be controlled. Numerical models are needed to further explore the relationships and feedbacks between processes that contribute to welding.

Keywords: volcanology; welding; compaction; pyroclastic; summary

1. Introduction

Welding in volcanology is expressed by dramatic variations in the texture, structure and physical properties of fragmental deposits (e.g., Smith, 1960a,b, 1979; Ross and Smith, 1961; Ragan and Sheridan, 1972; Peterson, 1979; Streck and Grunder, 1995; Quane and Russell, 2004). The welding process causes densification of volcanic deposits through deformation mechanisms including compaction and viscous flow which includes sintering (adhesion of molten fragments) and deformation of glassy clasts (e.g., Smith, 1960b; Guest and Rogers, 1967; Riehle et al., 1995). Despite decades of description and sporadic theoretical and experimental exploration (Fig. 1), the significance and implications of welding in volcanic deposits remain elusive. Welding is influenced by the dynamic

* Corresponding author. Tel.: +1 541 737 1249; fax: +1 541 737 1200.
E-mail address: grundera@geo.orst.edu (A. Grunder).

0377-0273/$ - see front matter © 2004 Elsevier B.V. All rights reserved.
doi:10.1016/j.jvolgeores.2004.10.010

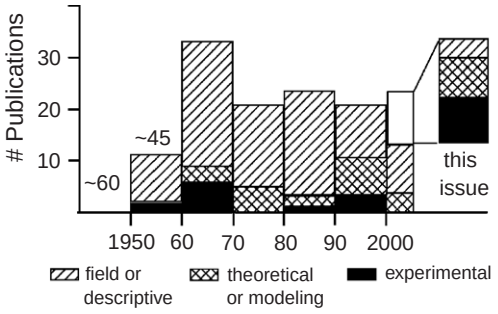

Fig. 1. Post-1950 publications on welding processes in volcanology summarized as histogram of number of publications by decade. The 1960s saw particularly abundant additions to the welding literature. Experimental, theoretical, and modeling studies are scarce relative to descriptive studies. The present volume (Welding Processes in Volcanology) includes papers in all three categories, but represents a particularly large advance in experimental and modeling papers. The numbers to the left of and above 1950 refer to descriptive papers on welded deposits from the first half of the century; many of these do not directly address welding. The compilation for post-1960 excludes several hundred publications that examine welded deposits but do not address the welding process itself. Sources include references cited by papers in this volume, the results of a detailed GEOREF search, plus the references in Smith's papers (1960a,b, 1979). Papers were grouped according to their main contribution; largely descriptive papers with important experimental or theoretical contributions were counted as half in each category. All publications are journal articles except for the B. Sc. thesis of Bierwirth (1982) and an abstract by Boyd and Kennedy (1951); both are included owing to the paucity of experimental literature.

interplay of diverse factors governing eruption, emplacement, and cooling processes.

Welded volcanic deposits, among which we include agglutinates, are geographically and temporally pervasive on Earth (e.g., Cook, 1959) and are also interpreted to occur on other planetary bodies (e.g., Mars: Crown and Greeley, 1993; and Io: McEwen et al., 2000). Most welding studies have focused on silicic ignimbrites; however, welding features are reported in diverse deposits, including pyroclastic flow (Smith, 1960a,b; Boyd, 1961) and fall (e.g., Sparks and Wright, 1979) deposits, spatter-fed lavas (e.g., Wolff and Sumner, 2000; Gottsman and Dingwell, 2001), bases and margins of lava flows (Naranjo et al., 1992; Sparks et al., 1993), and volcanic conduits (Kano et al., 1997; Tuffen et al., 2003). Welding is also recorded in deposits of virtually every magma composition from rhyolite to basalt and even carbonatite (e.g., Barker and Nixon, 1983). Welding is especially prevalent in deposits of peralkaline composition which also commonly exhibit signs of rheomorphic flow (e.g., Schmincke and Swanson, 1967; Wolff and Wright, 1981; Kobberger and Schmincke, 1999).

The collection of papers presented here derives largely from a special session *Welding Processes in Volcanology* organized for the 2003 meeting of AGU-EUG-EGS in Nice, France. Our intentions in convening the original conference session and in preparing this volume are to assess recent advances in understanding welding processes with a view towards developing new strategies for interpreting welding in volcanic deposits. We hope that these papers might initiate a renaissance in welding studies to rival the exceptionally productive decade of research heralded by Smith's landmark papers on welding in 1960 (Fig. 1). We note that the body of scientific literature on volcanoes has approximately quadrupled between the 1970s and 1990s (~13,000 versus 52,000 publication), so that the peak in activity on welding in the 1970s represents about 6 times (relative) the activity of the 1990s.

2. This volume

This issue brings together field, experimental, and modeling studies (Fig. 1). The field studies add new and important insights to an already substantial literature. In a field-based study of the Nuraxi Ignimbrite, Sicily, Pioli and Rosi (2005—this issue) use spatial distributions of textures, porosity, and paleomagnetic orientations to unravel a complicated history of pyroclastic flow, syn-emplacement welding, and rheomorphic and mass flow. A caution for paleovolcanological interpretations is provided by the work of Gifkins et al. (2005—this issue) who describe eutaxitic textures that are the result of diagenetic processes. They also provide criteria for distinguishing diagenetic compaction from welding compaction textures.

The experimental studies in this volume include work on analog and natural materials and explore the conditions conducive to densification and clast deformation. Sumner et al. (2005—this issue) consider agglutination and, particularly, clast morphology induced by impact in low-viscosity compositions. Through experiments on analog materials and com-

putational fluid dynamics, they describe impact outcomes for inviscid (such as basaltic) clasts. Quane and Russell (2005—this issue) explicitly explore the relationships between temperature, load, strain rate, and total strain in a series of high-temperature compaction experiments used to simulate welding. Their experiments control temperature and strain rate or load and are performed on spherical glass beads; results are used to develop a rheological model for strain accumulation during welding. Experiments on natural rhyolitic ash by Grunder et al. (2005—this issue) explore the effects of water and time on compaction, fabric development and clast deformation and the occurrence of vapor-phase crystallization. Giordano et al. (2005—this issue) provide the first glass transitions temperatures (T_g) determined for a range of natural hydrous glass compositions. T_g serves as a useful and accessible proxy for viscosity and separates the thermal regime into one dominated by viscous deformation ($T>T_g$) where adhesion and deformation of clasts operate on a relatively rapid time scale, versus a regime ($T>T_g$) where viscous flow would require excessive amounts of time.

The volume also contains two computational modeling studies which make contributions beyond the seminal works of Riehle (1973); Miller (1990), and Riehle et al. (1995). Sheridan and Wang (2005—this issue) present a model that allows for compaction-induced changes in thickness during cooling. They use the modeling to constrain average welding times, as well as the temporal implications of breaks between cooling units, by comparing modeled density profiles of the Bishop Tuff with field data. Keating (2005—this issue) investigates the effects of water, particularly vapor derived from the substrate during cooling of an ignimbrite. His model provides a vehicle for exploring the role of water vapor in causing secondary explosions, in promoting cooling, in enhancing welding by absorption into the glass, and in affecting devitrification and vapor-phase crystallization. Lastly, Russell and Quane (2005—this issue) use an inverse modeling approach in the interpretation of physical property data collected on samples from the Bandelier Tuff. The field data provide estimates of cumulative strain due to welding and are inverted through a rheological model to establish the relative roles of mechanical compaction versus viscous deformation. Russell and Quane conclude with a pair of dimensionless numbers, which are used to define the notion of a "welding window", that is, a combination of conditions under which welding is enhanced.

2.1. Quo vadimus?

There are several themes that emerge from this compilation which suggest fruitful avenues for further research. An abbreviated list follows.

(A) What are the mechanisms of welding and how do the relative roles of these mechanisms (e.g., mechanical compaction vs. viscous flow) vary in response to load, emplacement and thermal history, and melt properties (e.g., Russell and Quane; Giordano et al.; Grunder et al.)?

(B) What are the time scales of welding and how do they relate to internal (e.g., temperatures, melt properties, water content) and external (load, water infiltration) factors (Pioli and Rosi; Quane and Russell; Grunder et al.; Sheridan and Wang; Keating)?

(C) What are the effects of intrinsic versus extrinsic water on the welding history of pyroclastic rocks? Dissolved water has the potential of greatly enhancing welding (Giordano et al.; Grunder et al.; Russell and Quane) or can provide a pore-fluid pressure that inhibits compaction rates (Keating; Sheridan and Wang; Grunder et al.). Water or steam derived from a wet substrate or from rain or internally will affect cooling and welding (Keating).

(D) What morphological, textural, or physical attributes of a deposit are most important to measure in the field to facilitate interpretation of the welding history? In particular, what field observations are most useful and reliable for connecting field-based interpretations to the knowledge-base gathered from experimental and theoretical studies (Gifkins et al.; Pioli and Rosi; Russell and Quane; Sumner et al.)?

(E) What are the feedbacks among factors affecting welding? For example, how does permeability (connected pore space) vary spatially and temporally during welding of pyroclastic deposits and how is permeability evolution controlled by the welding history (e.g., high vs. low strain rates)? Does welding history and permeability

evolution affect the ultimate character of the welded deposit?

Below, we briefly expand our discussion on two of these topics, namely: the measurement of strain and the role of water.

3. Discussion

Welding in pyroclastic deposits results from a favorable intersection of: (1) the emplacement conditions of the deposit (i.e., eruptive temperature, column height, emplacement temperature, accumulation rate, thickness, or load); (2) the physical properties of the materials, including composition and water content (which together with temperature are subsumed in viscosity), T_g, particle size and shape, and sorting; and (3) dynamic feedbacks during welding and compaction involving changes in porosity and permeability, evolution of steam and absorption (or resorption) of water, devitrification, or vapor-phase alteration (see summaries by Smith, 1960a,b; Guest and Rogers, 1967; Riehle et al., 1995; Sparks et al., 1999). Among the many parameters and processes that need to be understood in order to deconvolve the welding signal in rocks, we focus on two issues: (1) identifying common metrics for comparison among field, experimental, modeling, and theoretical studies; and (2) the systematic investigation of the changes in and effects of water pressure during welding.

3.1. Measurement of strain

The welding intensity of pyroclastic deposits, as measured by changes in texture, structure, physical properties, typically varies with stratigraphic, and lateral position. Sheridan and Wang (2005—this issue) provide a brief summary of the sequence of events attending the compaction and welding of ash flow tuffs. The absolute changes in welding intensity can be tracked by converting the physical properties into corresponding values of strain (e.g., Smith and Bailey, 1966; Ragan and Sheridan, 1972; Sheridan and Ragan, 1976; Peterson, 1979; Sparks and Wright, 1979; Kobberger and Schmincke, 1999). Estimates of total strain also provide a common basis for relating field-based observations directly to results from laboratory or computational experiments (e.g., Quane et al., 2004). We note, however, that field studies that allow for the systematic analysis of strain due to welding are few.

The strain accumulating during progressive welding is mainly expressed as porosity loss (i.e., volume strain) via mechanical compaction and viscous deformation of the porous clastic matrix and vesicular particles. Thus, the thickness of the deposit, the bulk properties such as porosity and density, the axial ratios of clasts, and the degree of foliation can all serve as records of strain when compared with the unstrained (nonwelded) state (e.g., Sheridan and Ragan, 1976; Peterson, 1979; Sparks and Wright, 1979; Quane and Russell, 2004).

Using axial ratios of fiamme, shard elongation, or changes in Y-shard angle as metrics of strain can be complicated because the original shape of particles may not be known and the particles may become preferentially aligned during emplacement (e.g., Sheridan and Ragan, 1976; Peterson, 1979; Sparks and Wright, 1979). Although fiamme are the most conspicuous feature to measure in the field, they may exhibit a greater degree of deformation than the ash matrix (Ragan and Sheridan, 1972), reflecting greater initial porosities, incomplete vesiculation during eruption, or, as suggested by Sparks et al. (1999), lowering of viscosity by resorption of water sequestered in vesicles.

Using combinations of strain measurements allows for distinguishing between mechanical versus viscous deformation regimes. Coupling of density measurements and strain as measured from Y-shards and fiamme shape, in the Bishop Tuff, led Ragan and Sheridan (1972) to conclude that volume strain was dominant and that fiamme axial ratios (length over width) of 25 could result from volume loss alone. In contrast, substantial decoupling of the degree of flattening of fiamme and density in the Apache Leap Tuff caused Peterson (1979) to conclude that substantial “plastic flow” drove deformation at constant volume.

Porosity and density are strongly coupled bulk properties but can become uncoupled by variations in crystal or lithic content, heterogeneous glass compositions, and syn- or post-emplacement devitrification and alteration. They generally serve as excellent measures of strain until virtually all porosity is lost.

On the other hand, once porosity reduction is complete, most of the conventional metrics that are used to record volume strain are no longer useful for tracking continued strain (e.g., strain accompanying rheomorphic flow).

Volume strain can be expected to dominate until porosity has been reduced substantially (e.g., <5%) after which strain can be accommodated via (near-) constant volume deformation processes involving the pure viscous flow of the deposit or portions of the deposit, if strain becomes localized. Deformation under the constant volume constraint (e.g., zero porosity) can be via coaxial, pure shear as would attend the 2-dimensional flattening, or compaction of the deposit. Alternatively, constant volume strain can involve non-coaxial shear. For example, where pyroclastic deposits rest on a substantial slope, overburden loads can be resolved into non-coaxial shear stresses (e.g., simple shear) inducing strain manifest as rheomorphic flow (Wolff and Wright, 1981; Quane et al., 2004).

More explicit treatments of strain and constraints on strain rates are important next steps to link field data with models, experiments and the physical properties (viscosity and T_g) that bear on interpreting welding in pyroclastic rocks. In particular, a greater understanding is needed of how strain is partitioned between matrix and clasts or becomes localized within the deposit as a function of welding history. Although field data can provide a detailed spatial distribution of accumulated strain, experimental work is providing rheological relationships among temperature, load and the strain rates attending sintering and compaction (e.g., Boyd and Kennedy, 1951; Boyd, 1961; Friedman et al., 1963; Bierwirth, 1982; Quane and Russell, 2005—this issue). At present, there are no direct means of recovering strain rate information on welding from field studies. However, future experimentation may identify markers, textures, or other features within pyroclastic deposits that could serve as indicators of strain rates during welding. In a similar manner, Rust et al. (2003) used analogue fluid dynamic experiments to show how bubble sizes and orientations can constrain magma velocity profiles in conduits during eruption.

3.2. Water

Water is a critical factor in welding because it strongly affects the viscous response of the melt (e.g., Giordano et al., 2005—this issue), as well as affecting the abundance of vesicles and the fluid pressure in pore spaces. Water is variably lost from the magma during eruption, and is variably retained or gained during emplacement and cooling (e.g., Dingwell et al., 1996; Sparks et al., 1999; Keating, 2005—this issue). If permeability is low, steam will be trapped and pore fluid pressure may inhibit welding or lead to explosion.

The only welding experiments in which fluid and load pressure were controlled independently throughout the experimental run are those of Friedman et al.

Table 1
Summary of observed and computed properties of compaction experiments on samples of Bandelier ash flow as reported by Friedman et al. (1963), including: temperature, fluid pressure (P_{H_2O}), run times (t_{Max}), water content (X_{H_2O}), and final porosity (ϕ_{Final}) of run products

T (°C)	P_{H_2O} (MPa)	X_{H_2O} (wt.%)	t_{Max} (min)	ϕ_{Final} (%)	ε_{Max}	ε'_{Max}	$\log_{10}$ (Pa s)	X_{Sat} (wt.%)
635	0	0.15	1000	0	0.50	$10^{-3.4}$–$10^{-6.4}$	13.4	0
635	0.171	0.25	5300	10	0.44	10^{-4}–10^{-7}	13.2	0.18
635	0.345	0.4	32000	10	0.44	$10^{-4.5}$–$10^{-7.5}$	12.9	0.24
635	1.03	0.6	10000	31	0.28	$10^{-4.7}$–$10^{-7.1}$	12.5	0.43
635	2.07	0.85	53000	41.5	0.15	$10^{-5.2}$–$10^{-8.1}$	12.1	0.61
735	0	0.1	320	0.8	0.49	$10^{-3.3}$–$10^{-6.8}$	11.5	0
735	0.172	0.15	530	0.3	0.50	$10^{-3.2}$–$10^{-6.5}$	11.4	0.16
735	0.345	0.3	1750	1	0.49	$10^{-3.4}$–$10^{-6.9}$	11.2	0.21
735	1.03	0.5	3200	2	0.49	$10^{-3.7}$–$10^{-6.9}$	10.8	0.38
735	2.07	0.65	32000	4	0.48	$10^{-4.6}$–$10^{-7.4}$	10.6	0.56

Calculated properties include volume strain (ε), strain rate (ε'), melt viscosity (calculated according to Shaw, 1972) and the model solubility of H_2O in the melt (calculated according to Newman and Lowenstern, 2002). All experiments were performed on unsieved ash-sized mixtures of glass shards and pumice with 2–5% crystals under a load pressure of 3.6 MPa and having an initial porosity of 50%.

(1963). Their seminal work on the rhyolitic Bandelier Tuff is the basis for the ash densification function developed by Riehle (1973) which has been incorporated in subsequent ignimbrite cooling models (e.g., Riehle et al., 1995). Here we review these experiments for the purposes of stimulating further research on this important issue.

Friedman et al. (1963) conducted compaction experiments on samples of Bandelier ash using a fixed temperature (635 and 735 °C), a constant load pressure (3.63 MPa) and a constant water pressure of 0, 0.172, 0.345, 1.03, or 2.07 MPa (Table 1). The samples were held at the experimental temperature and P_{H_2O} for 1–2 days prior to applying the load. The experiments involved applying the fixed load and recording the shortening (porosity reduction) as a function of time (Fig. 2A,B). As noted by Sparks et al. (1999), the curves in the original graphs are mislabelled (reversed) in terms of P (e.g., Friedman et al., 1963: in Fig. 5 the curve labelled 20.7 bars P_{H_2O}

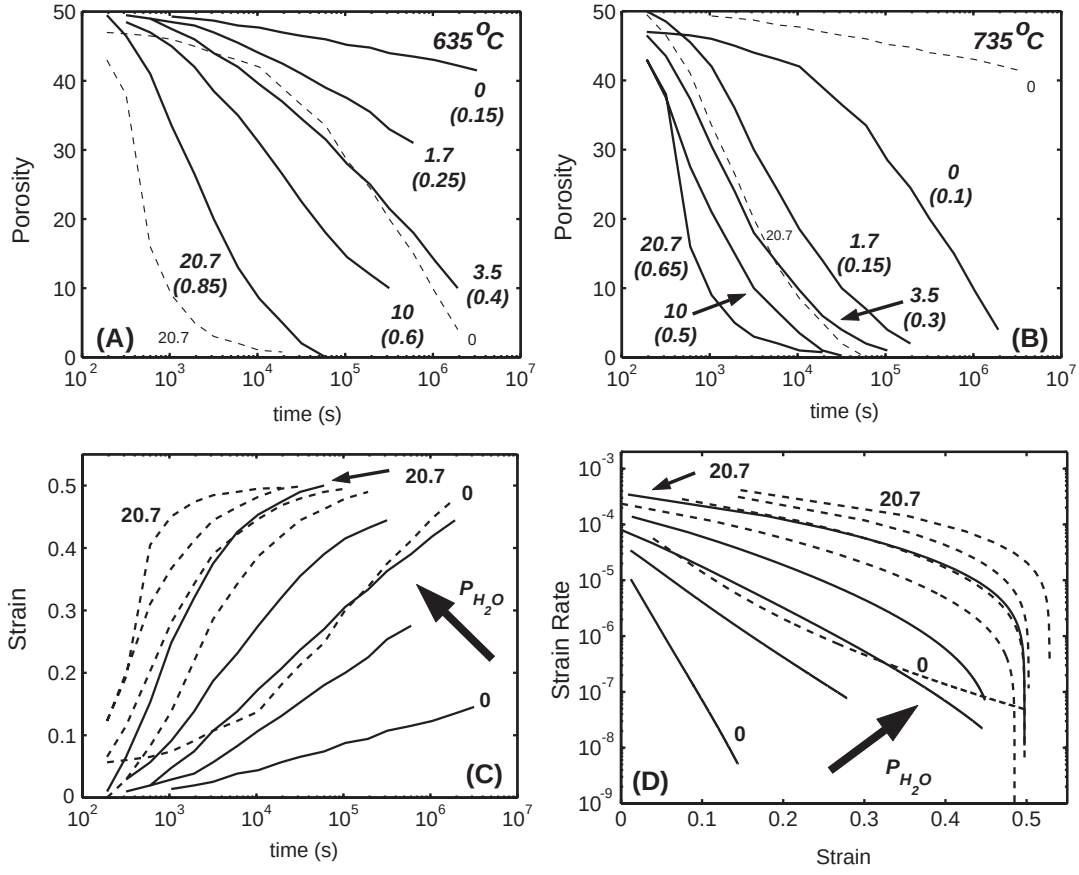

Fig. 2. Summary of high-temperature compaction experiments on ash from the Bandelier ash-flow tuff performed by Friedman et al. (1963). Experimental data sets (Table 1) are relabeled for the correct water pressures as pointed out by Sparks et al. (1999). (A) Results of experiments performed at 635 °C (solid lines) plotted as sample porosity vs. duration of experiment. The applied load is 36 bars (3.6 MPa) and the curves are labelled with the imposed P_{H_2O} (bars); measured water contents of samples are given in brackets. Dashed lines are 735 °C experiments under the same load pressure and the maximum and minimum water pressures (bars) taken from (B). (B) Results of experiments performed at 735 °C. Dashed lines are 635 °C experiments under the same load pressure and the maximum and minimum water pressures (bars) taken from (A). (C) Experimental data from (A) and (B) are summarized in terms of volume strain computed from porosity: solid lines denote 635 °C and dashed lines 735 °C. All porosity is lost where strain approaches 0.5; tangents to curves define operational strain rates. (D) The same experimental results summarized as calculated strain rates vs. strain. Experimental conditions are constant during each experiment, but strain rates are time dependent and strongly controlled by porosity loss (e.g., strain); implied deformation rates are highest when porosity is high (10^{-3} to 10^{-5}) and decrease rapidly as porosity disappears (10^{-6} to 10^{-8}).

should be labelled 0 bars P_{H_2O} and so on). The original data are replotted in Fig. 2A and B with corrected labels denoting P_{H_2O} and the measured water contents of the experimental run products. Increasing water pressure resulted in increased dissolved H_2O in the melt and greatly facilitates compaction. At 635 °C, in the experiment having a water pressure of 2.07 MPa, the sample lost all of its porosity, whereas in the experiments with lower P_{H_2O}, the samples maintained at least 10% porosity even after 5 days (Fig. 2A). In the higher-temperature experiments (Fig. 2B), samples compacted more quickly; in the high-water pressure experiments, samples reached zero porosity in just over 3 h.

The experimental results are summarized in terms of the volume strain (Fig. 2C) calculated from porosity and assuming a fixed original porosity (e.g., 50%). These strain/time curves directly record the evolution of strain rate during the separate experiments (Fig. 2D). The highest strain rates occur early when porosity in the sample is high and decrease steadily as porosity is reduced. Lastly, we have converted the computed strain rates to apparent viscosity to demonstrate the evolution of rheology during the compaction experiments (Fig. 3). Apparent viscosity increases steadily with porosity loss from the initial values of $10^{10–11}$ Pa s and $10^{9.5–10}$ Pa s for 635 °C and 735 °C, respectively.

It is important to note that all of Friedman et al.'s (1963) viscosity values are estimates made by comparing the compaction curves of the hydrous ash with the corresponding compaction curves for ash-sized powders of dry pyrex of known viscosity. However, analysis of the compaction curves for the pyrex powders implies substantially higher viscosities than were measured on the corresponding pyrex melts. This discrepancy may result from experimental problems, such as strain being partitioned into the experimental apparatus or into the sample holder, or from frictional effects on one of the two pistons.

These experiments demonstrate the relative roles of temperature, P_{H_2O}, and pore fluid pressure. Increased temperature promotes higher strain rates and greater degrees of compaction due to lowering of viscosity. When P_{H_2O} is increased, the melt becomes increasingly hydrous which lowers the viscosity, thereby

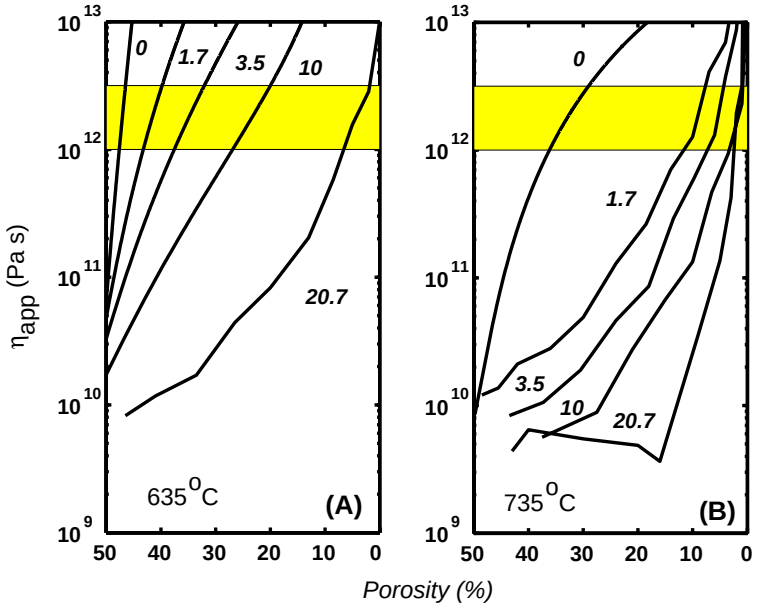

Fig. 3. The same experimental data sets (Friedman et al., 1963; Table 1; Fig. 2) are portrayed as apparent viscosity (η_{app}) vs. porosity for (A) 635 °C and (B) 735 °C. Apparent viscosity of the sample is computed from rates of porosity loss assuming that all deformation is accommodated by viscous flow. Curves are labelled by P_{H_2O}; experiments with higher P_{H_2O} have melts with higher H_2O contents and describe paths having low effective viscosities. Values of η_{app} increase as porosity is lost. Grey bars denote the range of viscosities coincident with the calorimetric glass transition (10^{12}–$10^{12.5}$ Pa s).

causing a substantial increase in strain rates and total compaction (Table 1). Based on coincidence among calculated strain rate curves, a temperature increase of 100 °C has a similar effect to adding 0.3 wt.% H_2O to 0.55 wt.% H_2O to the melt (Fig. 2D). The role and evolution of pore fluid pressure is uncertain in these experiments because the nature and distribution of the fluid phases are not well characterized. After dwell times of 10 s of hours at elevated temperature and several bars of P_{H_2O}, the melt should be saturated with H_2O and in equilibrium with a fluid phase. The solubility of water in rhyolite derived by Friedman et al. (1963) is greater than that based on the solution model of Newman and Lowenstern (2002; Table 1). We suggest that some water may have been trapped in isolated pores during the experiments as the ash became sintered; some of the sintering and trapping of fluid may have occurred prior to application of the experimental load (e.g., during the dwell time). If so, the compaction experiment will have had an effective load that is less than the 3.63 MPa load pressure ($P_{eff}=P_{load}-P_{H_2O}$).

In natural deposits undergoing welding, we expect porosity and permeability evolution to be highly variable and critical to the nature, style and time scales of welding (e.g., Sparks et al., 1999; Keating, 2005—this issue). The effects of permeability on the distribution and intensity of welding have seen little attention and are likely line of pursuit. We suggest that a new generation of hydrous compaction experiments are in order to take us past the exceptional work of Friedman et al. (1963).

4. Conclusion

The papers collected in this volume represent a significant advance in understanding welding in volcanology and point to future lines of inquiry. In the realm of field and textural studies, more systematic and quantitative studies are necessary to evaluate strain histories related to welding and the timing of welding relative to other processes during eruption and emplacement. A new generation of experiments is needed in which load, strain rate and volatile pressure can be controlled. Numerical models are needed to further explore the relationships and feedbacks between processes that contribute to welding.

Acknowledgements

We thank the contributors to the volume for taking part in this endeavor and bearing with our underdeveloped editorial skills. In this regard, we greatly appreciate the encouragement and support of Friso Veenstra and Patricia Massar at Elsevier. The original special session that was convened at the Nice meeting of AGU-EUG-EGS was made possible by the support of Don Dingwell and we thank those who participated in that session. We especially acknowledge the reviewers who contributed with abundant insight and tact to making this a better volume: Mike Branney, Ray Cas, Bob Christiansen, Cathy Busby, Armin Freundt, Jim Gardner, Jenny Gilbert, Daniele Giordano, Joachim Gottsmann, Bruce Houghton, Gordon Keating, Ian Skilling, Martin Streck, Don Swanson, Thor Thordarson, Hugh Tuffen, Alan Whittington and John Wolff; Jocelyn McPhie and Steve Sparks reviewed this introduction to the volume. Lastly, we thank Steve Quane and Alison Rust for critical and engaging discussions.

References

Barker, D.S., Nixon, P.H., 1983. Carbonatite lava and welded air fall tuff, Fort Portal field, Western Uganda. Eos, Trans.-Am. Geophys. Union 64, 896.

Bierwirth, P.N., 1982. Experimental welding of volcanic ash. Unpubl. BSc Hons. thesis, Monash University.

Boyd, F.R., 1961. Welded tuffs and flows in the rhyolite plateau of Yellowstone Park, Wyoming. Geol. Soc. Am. Bull. 72, 387–426.

Boyd, F.R., Kennedy, G.C., 1951. Some experiments and calculations relating to the origin of welded tuffs. Trans. Geophys. Union 32, 327–328.

Cook, E.F., 1959. Ignimbrite bibliography. Idaho Bur. Mines Geol. Info. Circ. 4, 30 pp.

Crown, D.A., Greeley, R., 1993. Volcanic geology of Hadriacapatera and the eastern Helles region of Mars. J. Geophys. Res.-Planets 98, 3431–3451.

Dingwell, D.B., Romano, C., Hess, K.U., 1996. The effect of water on the viscosity of haplogranite melt under P-T-X conditions relevant to silicic volcanism. Contrib. Mineral. Petrol. 124, 19–28.

Friedman, I., Long, W., Smith, R.L., 1963. Viscosity and water content of rhyolite glass. J. Geophys. Res. 68, 6523–6535.

Gifkins, C.C., Allen, R.L., McPhie, J., 2005. Apparent welding textures in altered pumice-rich rocks. J. Volcanol. Geotherm. Res. 142, 29 –47.

Giordano, D., Nichols, A.R.L., Dingwell, D.B., 2005. Glass transition temperatures of natural hydrous melts: a relationship

with shear viscosity and implications for the welding process. J. Volcanol. Geotherm. Res. 142, 105–118.
Gottsman, J., Dingwell, D.B., 2001. Cooling dynamics of spatter-fed phonolite obsidian flows on Teneriefe, Canary Islands. J. Volcanol. Geotherm. Res. 105, 323–342.
Grunder, A.L., Laporte, D., Druitt, T.H., 2005. Experimental and textural investigation of welding: effects of compaction, sintering, and vapor-phase crystallization in the rhyolitic Rattlesnake Tuff. J. Volcanol. Geotherm. Res. 142, 89–104.
Guest, J.E., Rogers, P.S., 1967. The sintering of glass and its relationship to welding in ignimbrites. Proc. Geol. Soc. London 1641, 174–177.
Kano, K., Matsuura, H., Yamauchi, S., 1997. Miocene rhyolitic welded tuff infilling a funnel-shaped eruption conduit Shiotani, southeast of Matsue, SW Japan. Bull. Volcanol. 59, 125–135.
Keating, G.N., 2005. The role of water in cooling ignimbrites. J. Volcanol. Geotherm. Res. 142, 145–171.
Kobberger, G., Schmincke, H.U., 1999. Deposition of rheomorphic ignimbrite D (Mogan Formation) Gran Canaria, Canary Islands, Spain. Bull. Volcanol. 60, 465–485.
McEwen, A.S., et al., 2000. High-resolution views of Jupiter's moon Io. Science 288 (5469), 1193–1198.
Miller, T.F., 1990. A numerical model of volatile behavior in nonwelded cooling pyroclastic deposits. J. Geophys. Res. 95, 19349–19364.
Naranjo, J.A., Sparks, R.S.J., Stasiuk, M.V., Moreno, H., Ablay, G.J., 1992. Morphological, textural and structural variations in the 1988–1990 andesite lava of Lonquimay. Geol. Mag. 129, 657–678.
Newman, S., Lowenstern, J.B., 2002. VolatileCalc: a silicate melt–H_2O–CO_2 solution model written in Visual Basic for Excel. Comput. Geosci. 28, 597–604.
Peterson, D.W., 1979. Significance of flattening of pumice fragments in ash-flow tuffs. In: Chapin, C.E., Elston, W.E. (Eds.), Ash-Flow Tuffs and Associate Igneous Rocks. Spec. Pap. Geol. Soc. Am. 180, 195–204.
Pioli, L., Rosi, M., 2005. Rheomorphic structures in a high-grade ignimbrite: The Nuraxi tuff, Sulcis volcanic district (SW Sardinia, Italy). J. Volcanol. Geotherm. Res. 142, 11–28.
Quane, S.L., Russell, J.K., 2004. Ranking welding intensity in pyroclastic deposits. Bull. Volcanol., Online First, 1432–0819.
Quane, S.L., Russell, J.K., 2005. Welding: insights from high-temperature analogue experiments. J. Volcanol. Geotherm. Res. 142, 67–87.
Quane, S.L., Russell, J.K., Kennedy, L.A., 2004. A low-load high-temperature deformation apparatus for volcanological studies. Am. Mineral. 89, 873–877.
Ragan, D.H., Sheridan, M.F., 1972. Compaction of the bishop Tuff, California. Geol. Soc. Am. Bull. 83, 95–106.
Riehle, J.R., 1973. Calculated compaction profiles of rhyolitic ash-flow tuffs: computational model. Bull. Volcanol. 57, 319–336.
Riehle, J.R., Miller, T.F., Bailey, R.A., 1995. Cooling, degassing and compaction of rhyolitic ash-flow tuffs: a computational model. Bull. Volcanol. 57, 319–336.
Ross, C.S., Smith, R.L., 1961. Ash-flow tuffs: their origin, geologic relations, and identification. U.S. Geol. Surv. Prof. Pap. 366, 81 pp.
Russell, J.K., Quane, S.L., 2005. Rheology of welding: inversion of field constraints. J. Volcanol. Geotherm. Res. 142, 173–191.
Rust, A.R., Manga, M., Cashman, K.V., 2003. Determining flow type, shear rate and shear stress in magmas from bubble shapes and orientations. J. Volcanol. Geotherm. Res. 122, 111–132.
Schmincke, H.U., Swanson, D.A., 1967. Laminar viscous flowage structures in ash-flow tuffs from Gran Canaria, Canary islands. J. Geol. 75, 641–664.
Shaw, H.R., 1972. Viscosities of magmatic silicate liquids: an empirical model of prediction. Am. J. Sci. 272, 438–475.
Sheridan, M.F., Ragan, D.M., 1976. Compaction of ash-flow tuffs. In: Chilingarian, G.V., Wolf, K.H. (Eds.), Compaction of Coarse-Grained Sediments, vol. II. Elsevier, Amsterdam, Netherlands, pp. 677–717.
Sheridan, M.F., Wang, Y., 2005. Cooling and welding history of the Bishop Tuff in Adobe Valley and Chidago Canyon, California. J. Volcanol. Geotherm. Res. 142, 119–144.
Smith, R.L., 1960a. Ash-flows. Geol. Soc. Am. Bull. 71, 795–842.
Smith, R.L., 1960b. Zones and zonal variations in welded ash-flows. U.S. Geol. Surv. Prof. Pap. 354-F, 149–159.
Smith, R.L., 1979. Ash-flow magmatism. In: Chapin, C.E., Elston, W.E. (Eds.), Ash-Flow Tuffs. Spec. Pap. Geol. Soc. Am. 180, 5–27.
Smith, R.L., Bailey, R.A., 1966. The Bandelier Tuff: a study of ash-flow eruption cycles from zoned magma chambers. Bull. Volcanol. 29, 83–103.
Sparks, R.S.J., Wright, J.V., 1979. Welded air-fall tuffs. In: Chapin, C.E., Elston, W.E. (Eds.), Ash-Flow Tuffs. Spec. Pap. Geol. Soc. Am. 180, 155–166.
Sparks, R.S.J., Stasiuk, M.V., Gardeweg, M., Swanson, D.A., 1993. Welded bressias in andesite lavas. J. Geol. Soc. (London) 150, 897–902.
Sparks, R.S.J., Tait, S.R., Yanev, Y., 1999. Dense welding caused by volatile resorption. J. Geol. Soc. (London) 156, 217–225.
Streck, M.J., Grunder, A.L., 1995. Crystallization and welding variations in a widespread ignimbrite sheet; the Rattlesnake Tuff, eastern Oregon, USA. Bull. Volcanol. 57, 151–169.
Sumner, J.M., Blake, S., Matela, R.J., Wolf, J.A., 2005. Spatter. J. Volcanol. Geotherm. Res. 142, 49–65.
Tuffen, H., Dingwell, D.B., Pinkerton, H., 2003. Repeated fracture and healing of silicic magma generate flow banding and earthquakes? Geology 31, 1089–1092.
Wolff, J.A., Sumner, J.M., 2000. Lava fountains and their products. In: Sigurdson, H. (Ed.), Encyclopedia of Volcanoes. Academic Press, pp. 321–329.
Wolff, J.A., Wright, J.V., 1981. Rheomorphism of welded tuffs. J. Volcanol. Geotherm. Res. 10, 13–34.